Targeted protein degradation of phospholamban for PLN treatment

Sabine van Bentum

Targeted protein degradation of phospholamban for PLN treatment
Major research internship| Written report
University Medical Centre Utrecht | Experimental Cardiology
September 2022 – Augustus 2023

Sabine C. van Bentum
6426557
Biology of Disease
Utrecht University

Supervisors
Daily supervisor: Jort van der Geest
Examiner: Dr. Zhiyong Lei
Second examiner: Dr. Vasco Sampaio Pinto

Image source: Self made

Table of content

Layman's Summary

Phospholamban is a protein in heart cells. The protein has a regulatory function in the working of the heart. Some people have a mistake in the genetic code (also called mutation) of the phospholamban protein. Due to this mutation the protein cannot function properly, this can result in a heart disease. People with this specific heart disease get standard heart failure care. The aim of this treatment is to reduce symptoms. However, at this moment it is not possible to cure the disease. To try to make it possible to cure this disease we have set up this research project. During this project we tried to make a so-called fusion protein, which is a protein which is fused to something else. Our fusion protein consists of an E3 ligase (protein part) and a nanobody against the phospholamban protein. The E3 ligase is a protein which has a role in the protein degradation of the cell. A nanobody is a special kind of antibody which can be derived from llamas. Llamas produce the nanobody if they are injected with the protein wherefore you want nanobodies. This injected protein will be recognized as foreign which result in the production of nanobodies. We first tried to let a llama produce the nanobody for us but that failed. We think that it failed due to the fact that the phospholamban protein of the lama looks very much the same as that of the human, and that the llama did not recognize it as a foreign protein. Therefore, another approach was needed to make the nanobody. In the literature, a synthetically (in the lab) produced nanobody, called VHHB4, is described. This nanobody is able to bind to the healthy phospholamban protein, and we wanted to know if this nanobody is also able to bind to the phospholamban protein with the mutation. We were able to confirm that this is indeed the case, moreover we showed that VHHB4 did not bind better to the healthy or mutated version of the protein. Because the VHHB4 nanobody was able to bind the mutated phospholamban, we decided to use this VHHB4 nanobody for the production of our fusion protein. After we produced our fusion protein, we tested it in cells if the fusion protein is able to reduce the phospholamban levels and can improve the function of the cells. This data showed inconclusiveness and therefore it is hard to draw a conclusion. Because the used nanobody binds to the mutated phospholamban as good as the healthy phospholamban protein, it cannot be used to treat the genetic disease. So, to cure the heart disease another approach is needed.

Abstract

The phospholamban protein has an important role in the calcium regulation of the cardiomyocytes. Deletion of the 14th arginine (PLN_R14del) can lead to dilated cardiomyopathy with ventricular extra systolic beats and ventricular tachycardia episodes. The pathophysiology of the PLN_R14del cardiomyopathy is not exactly known and a disease specific treatment is not available yet. A potential treatment for the disease is nanobody assistant targeted protein degradation of the PLN protein, whereby a nanobody is fused to the Von Hippel-Lindau (VHL) E3 ligase. The first approach to get a PLN nanobody was llama immunization with the PLN protein, however it did not lead to the production of nanobodies. It is thought that this is caused by the fact that the protein is highly conserved. Literature showed that the synthetically produced VHHB4 nanobody has affinity for the PLN_WT protein, and we have confirmed that this nanobody also has affinity for the PLN_R14del protein. Therefore, it can be used for the production of the fusion protein. The VHHB4_VHL sequence was successfully molecular cloned by *Escherichia Coli*. HEK_Trex cells and induced pluripotent stem cell derived cardiomyocytes (iPSC-CMs) were transfected with this VHHB4_VHL construct. After transfection, the calcium handling of the iPSC-CMs is determined and the proteins of the HEK_Trex cell and iPSC-CM lysates is analyzed. The protein data as well as the functionality data are inconclusive, so we still do not know if our VHHB4_VHL fusion protein is able to perform targeted degradation.

1. Introduction

Calcium (Ca^{2+}) is one of the most accomplished biological messenger molecules. It functions in many biological activities such as muscle contraction, cellular exocytosis, and neural activity[1]. Furthermore, Ca^{2+} is required for the contraction of the heart and therefore decent cardiac Ca^{2+} handling is required[2].

Depolarization of the cardiomyocyte results in the influx of Ca^{2+} to the cytosol. The Ca^{2+} binds to ryanodine receptors (RyRs), stimulating the Ca^{2+} release out of the sarcoplasmic reticulum (SR). Thereafter, Ca^{2+} binds to the myofibril which subsequently leads to the contraction of the cardiomyocyte. At the end of the contraction, the high cytosolic Ca^{2+} concentration leads to phosphorylation of phospholamban (PLN) at the seventeenth threonine (Thr17) by calmodulin-dependent protein kinase II (CaMKII) and phosphorylation at the sixteenth serine (Ser16) by active cyclic AMP-dependent Protein kinase A (PKA)[3,4].

The result of these phosphorylations is dissociation of PLN from sarco(endo)plasmic reticulum Ca^{2+} ATPase subtype 2a (SERCA2a). Consequently, SERCA2a is not inhibited and removes Ca^{2+} out of the cytosol to the SR (Figure 1)[3,4]. SERCA2a diminishes more than 70% of the cytosolic Ca^{2+}. Dephosphorylation of PLN at resting Ca^{2+} concentration, leads to an increased affinity of PLN for SERCA2a. This causes inhibition of SERCA2a and thereby decreased removing of Ca^{2+} out of the cytosol[4].

Dysfunction of proteins involved in cardiac Ca^{2+} handling lead to disturbance of Ca^{2+} handling and thereby to cardiomyopathy[5,6]. Dysfunctional RyR leads to depletion of SR Ca^{2+} stores and elevation of cytosolic Ca^{2+}, which increases the incidence of arrhythmias[6]. Decreased SERCA2a function or increased PLN function leads to cytosolic Ca^{2+} accumulation and prevents the relaxation of the cardiomyocyte. Moreover, the available SR Ca^{2+} concentration during the contraction is decreased[6]. The SERCA2a : PLN ratio is reduced during heart failure, which leads to an increased PLN function[7].

PLN consists of 52 amino acids and is highly conserved among different species[3,8]. Nevertheless, there are different mutations identified in the human PLN gene, which leads to the dysfunction of the PLN protein. Heterozygote replacement of leucine 39 to a stop codon (PLN_R39stop) leads to hypertrophy with normal contractile performance while homozygote expression leads to dilated cardiomyopathy and early death[9,10]. The ninth arginine is a mutation hotspot, it can be changed in for example cysteine (R9C), histidine (R9H), or leucine (R9L). These mutations may lead to dilated cardiomyopathy (DCM) and heart failure phenotype[11]. The fourteenth amino acid arginine (Arg14) is important for the upstream phosphorylation by PKA[12] and heterozygote deletion of this amino acid (PLN_R14del) can lead to DCM with ventricular extra systolic beats and ventricular tachycardia episodes. This progress to congestive heart failure by middle age and can lead to sudden cardiac death[13,14]. Not everyone who carries this mutation, develops symptoms[14].

The mechanisms of the PLN_R14del cardiomyopathy development are not completely understood[15]. The current theory is that heterozygous expression leads to the superinhibition of SERCA2a activity (Figure 1). This superinhibition theory has been shown in HEK_293 cells and is likely related to the structure of PLN_R14del which prevents the phosphorylation of it[13]. According to that study, the deletion of Arg14 partially disrupts the PLN pentamer's stability, leading to an increased concentration of the monomer and thereby leads to more inhibition of SERCA2a[13]. However, other studies show enhanced SERCA2a function in presents of PLN_R14del, so the loss of PLN inhibition[16,17]. Although it is not exactly known if the mutation leads to loss or gain of function of PLN, it is expected that the change in function contributes to myocardial Ca^{2+} dysregulation and the progression of heart disease[18].

The clinical presentation of PLN_R14 patients differs among them, and it is unclear why this can be so different[9]. Looking at heart histology of patient samples shows significantly higher fibrosis replacement[19,20]. The change in structure and function is present in both sides, left and right, of the heart [9]. Moreover, the ECGs show abnormal characteristics: a lower QRS-complex, a decreased R-wave[9,13,14], and an inverted T-wave are observed[9,21].

At this moment, a disease-specific treatment is not available for PLN_R14del patients. The treatment is based on regular heart failure treatment guidelines and reduces symptoms [21,22]. The treatment includes angiotensin-converting enzyme (ACE) inhibitors and beta-blockers[22]. If this is not

enough anymore, the options are an implantable cardio defibrillator, left ventricular assist device, and heart transplantation[21]. Thus, we require new treatment options for PLN_R14-del patients.
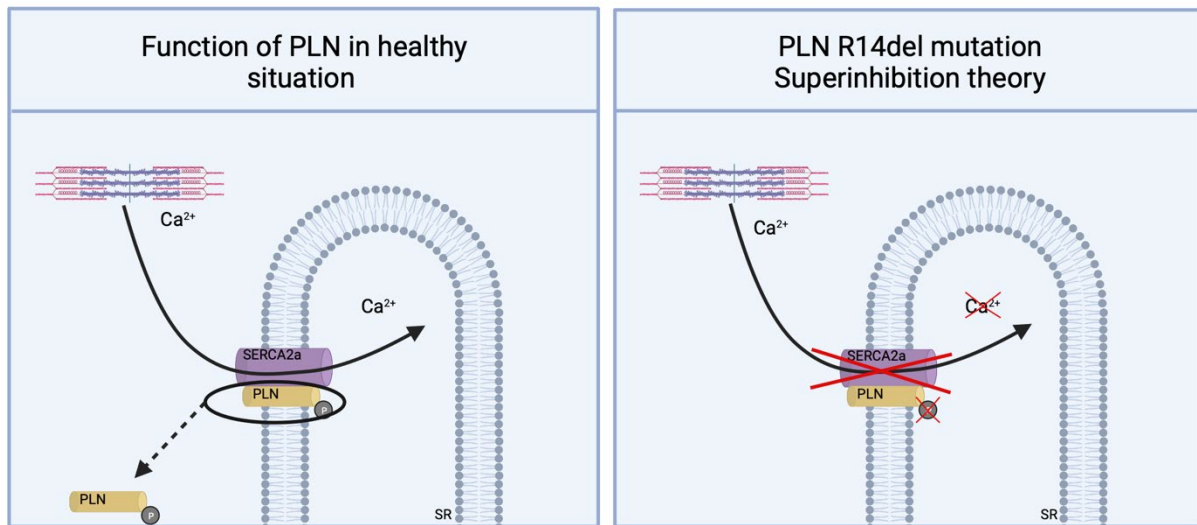

Figure 1 Function of WT phospholamban (PLN) and PLN arginine 14 deletion (PLN_R14del). After the contraction of a cardiomyocyte, sarco(endo)plasmic reticulum calcium ATPase subtype 2a (SERCA2a) transports the intracellular calcium (Ca²⁺) to the sarcoplasmic reticulum (SR). SERCA2a is inhibited by PLN at low cytosolic Ca²⁺ concentrations. Phosphorylation of PLN releases PLN from SERCA2a. The PLN_R14del mutation prevents the phosphorylation of the PLN_R14del protein. This prevents the release of PLN_R14del from the SERCA2a protein and thereby the transport of cytosolic Ca²⁺ to the SR.

Nanobodies, also called VHH, can be used as potential therapeutics[23]. They can be derived from heavy-chain-only antibodies (HCAbs) produced by camelids[24–26]. A nanobody has a complete antigen binding capacity and has a high specificity and affinity, comparable with a complete antibody[26,27]. The nanobody structure is almost similar to the structure of the variable domain of the heavy chain (VH domain) of conventional IgG antibodies[28].

Besides therapeutics, nanobodies can be used in research and diagnosis[23]. Nanobodies generally have a fast clearance and thus a short serum half-life[29]. This fast clearance is due to the better tissue penetration as a consequence of the small size of the nanobody[30]. Furthermore, nanobodies have a low immunogenicity[31]. These characteristics make nanobodies a promising tool[32]. The main applications of nanobodies in treatment are: inhibiting ligand-receptor interactions, keeping antigens in an inactive receptor state, and provoking receptor activation[29].

De Genst *et al.* found two nanobodies for the wildtype PLN (PLN_WT) protein, which they called VHHB4 and VHHC6[33]. With the use of a cardiac-specific adeno-associated virus 9 (AAV9) vector, this group was able to prolonged express the nanobody in cardiomyocytes. The VHHB4 nanobody binds to the non-phosphorylated as well as the Ser16 phosphorylated conformation of the PLN protein and leads to longer relaxation, without increase in Ca²⁺ transient amplitude in rat-derived cardiomyocytes. The VHHC6 nanobody only binds to the Ser16 phosphorylated PLN protein conformation and only has minor effects on Ca²⁺ kinetics in cardiomyocytes[33].

Targeted protein degradation (TPD) approaches are used to reduce the activity of specific cellular proteins by modification with degrons or adapting components of protein degradation machinery[34]. It is used to explore cellular pathways, to discover the function of proteins, and to use as a promising therapeutic approach [34–37]. This approach degrades targeted proteins within min to hours, which prevents cellular adaptations[35,36]. TPD can be reversible, and it can be controlled by chemical or physical stimulation by incorporating functional groups[35,36].

Most TPD strategies rely on the ubiquitin-proteasome system (UPS) which is a system that cells use to get rid of regulatory, damaged, and misfolded proteins via proteasomes[34,36]. The UPS consist of three major activities, one of them is the ubiquitin ligase (E3). E3 ligases are responsible for the recognition of the targeted protein, therefore this enzyme is mostly used for TPD [34]. There are over 600 different E3 ligases, an example is the Von Hippel-Lindau (VHL)[38]. By fusing a nanobody to E3 ligases as TPD strategy, the nanobody function as the recognition domain of the UPS. The fusion of

anti-GFP to a subtype of E3 ligases results in the degradation of GFP-tagged proteins in HEK293 cells[35,39]. Hence, the use of nanobodies in TPD approaches has a high potency. However, this technique is not yet explored in the heart or heart cells.

During this research project, I explore the effect of TPD on heart cells. Therefore, the VHHB4 fused to VHL is used to target and thereby remove the PLN protein in induced pluripotent stem cell-derived cardiomyocytes (iPSC-CMs)(Figure 2). We hypothesize that the elimination of the PLN_R14del protein using a VHL E3 protein fused to a PLN_R14del nanobody will relieve the cardiomyopathy phenotype associated with the mutation.

A llama was immunized with PLN to produce nanobodies. However, analysis of the llama serum showed absence of nanobodies. Therefore, the affinity of the synthetically produced VHHB4 and VHHC6 nanobodies for the PLN_R14del protein was tested. The VHHB4 showed affinity for the PLN_R14del and the PLN_WT protein. Hence, we decided to use this nanobody for our fusion protein, which consist of the nanobody and the VHL ligand. We amplify the ordered fusion protein sequence with the use of PCR and build them into Phage 2 vectors with the use of High Fidelity (HiFi) assembly. Next, bacteria are transformed with these vectors to amplify the vectors. Later, HEK_Trex cells are transfected with the VHHB4_VHL construct as a proof of concept. Where after the amount of PLN protein is analyzed. Although not all data confirmed it, it seems like transfection with our construct leads to targeted degradation. Therefore, we continued with a transfection of iPSC-CMs cell culture with the VHHB4_VHL construct. Followed by an analysis of the PLN protein and the function of iPSC-CMs via viability assay and Ca^{2+} measurements. The PLN protein data as well as the functionality data are inconclusive, so we still do not know if our VHHB4_VHL fusion protein is able to perform targeted degradation.
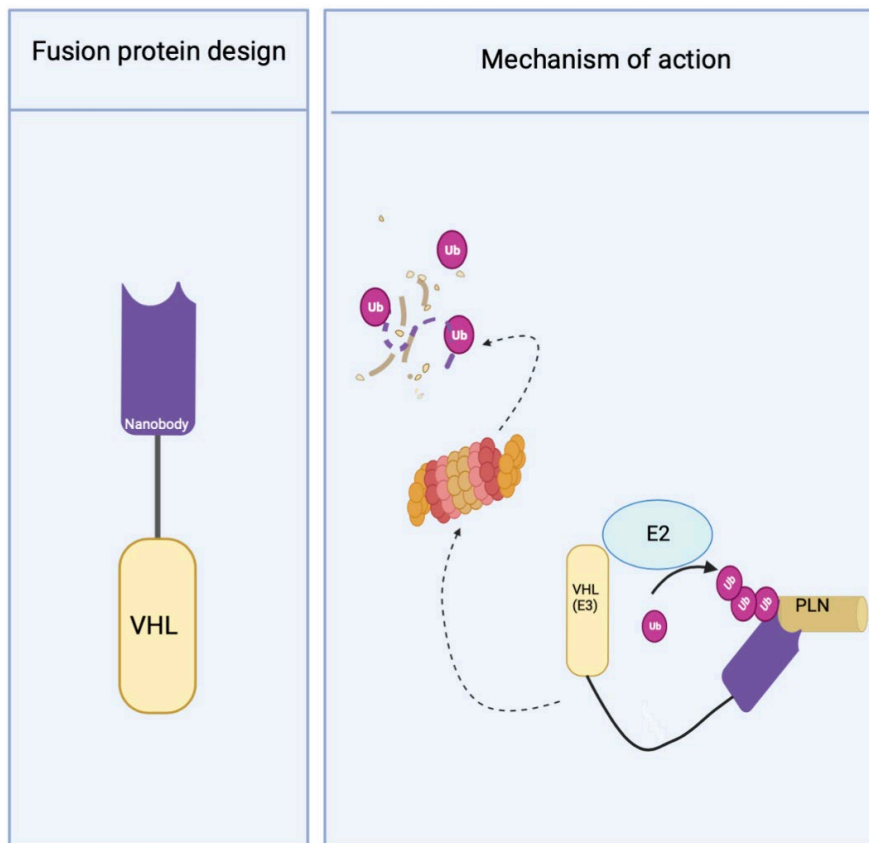

Figure 2 Overview of the targeted protein degradation approach of phospholamban (PLN). *First panel: an overview of the designed fusion protein. The adapted VHHB4 nanobody from de Genst et al. is fused to Von Hippel-Lindau (VHL) to target the PLN arginine14 deletion (PLN_R14del) protein. Second panel: the aim of this project is to use the fusion protein to target and degrade the PLN protein via the ubiquitin-proteasome system to prevent inhibition of the sarco endoplasmic reticulum calcium ATPase 2a (SERCA2a).*

2.   Materials and methods

2.1   Materials

Reagent or resource	Supplier	Identifier
Experimental models		
Escherichia coli strain stable 3		Custom
T-rex-293	Invitrogen	R78007
T-rex-293 expressing PLN_WT		Custom
T-rex-293 expressing PLN_R14del		Custom
Induced pluripotent stem cell derived cardiomyocytes D4		Custom
Induced pluripotent stem cell derived cardiomyocytes C31		Custom
Induced pluripotent stem cell derived cardiomyocytes NPO		Custom
Antibodies		
rabbit-anti-llama-imunoglobulin_G-VHH-Horseradish Peroxidase		
rabbit-anti-llama-IgG-VHH-Fluorescent		
Goat-anti-rabbit-HRP antibody	Dako	P0448
Goat-anti-PLN antibody	OriGene	TA311243
Mouse-anti-betatubulin	Invitrogen	MA5-16308
Donkey-anti-goat IrDye 800	Life/Licor	92632214
Donkey-anti-mouse IrDye 680	Odyssey	926-32222
Chemicals, Reagents and Recombinant Proteins		
Phosphate Buffered Saline- Sterile	Gibco	10010-015
RPMI-1640 Medium	Gibco	52400-025
DMEM Medium	Gibco	42430-025
PLN_WT protein		
PLN_R14del protein		
Taq buffer with $(NH_4)_2SO_4$(10x)	Thermo Scientific	01023505
dNTP mixture	TaKaRa	AIG2333A
25 mM $MgCl_2$	Thermo Scientific	00712595
Hot start Taq DNA polymerase	BioLabs	M0495L
Dimethyl sulfoxide	Sigma	D2650
NotI	BioLabs	R0189S
BamI High Fidelity	BioLabs	R3136M
rCutsmart	BioLabs	B6004S
6x TriTrack DNA Loading Dye	Thermo Scientific	R1161
Generuler 50 bp DNA Ladder, ready-to-use	Thermo Scientific	SM0373
1 Kb Plus DNA ladder	Invitrogen	10787-018
3-Methylbenzo[d]thiazol-2(3H)-ylidene)methyl)-1-propylquinolin-1-ium 4-methylbenzenesulfonate (SYBR safe) DNA Gel stain	Invitrogen	S33102
Agarose MP	Roche	11388991001
3,3',5,5'-tetramethuylbenzidine (TMB)	Sigma	SLBS5110

Nupage MOPS SDS running buffer (20x)	Invitrogen	NP0001-02
Intercept Blocking Buffer	Li-Cor	927-60001
Nucleospin Plasmid Quickpure kit	Machery-Nagel	740615.250
Nucleobond Xtra Maxi Plus EF kit	Machery-Nagel	740426.50
Nucleospin Gel and PCR Clean-up kit	Machery-Nagel	740609.250
Lipofectamin 3000	Thermo Scientific	L3000015
Lipofectamin RNAimax	Thermo Scientific	13778075
VHHB4 forward primer	IDT	Custom
VHHB4 reverse primer	IDT	Custom
VHHB4_VHL sequence	IDT	Custom
EF1a_seq_F1 sequence primer	IDT	Custom
Lentiviral backbone-pHAGE2-PuroR_MCS vector	IDT	Custom
Micro BCA™ protein assay kit	Thermo Scientific	23235

Equipment

T175 Culture flask	Sardedt	83.3911.502
6 well plate	Costar	3506
Nunc MaxiSorp™ _Flat-bottom	Thermo Scientific	439454
96-well Plate, Flat-bottom	Greiner	655161
Bolt™ Mini Gel tank	Life technologies	B4477599
Bolt™ 4-12% Bis-Tris Plus	Invitrogen	NW04125BOX
iBlot® 2 Dry Blotting system	Life technologies	IB21001
iBlot® 2 PVDF Regular stacks	Invitrogen	IB24001
Xpose touch and go	Trinean	
Multiskan FC	Thermo Scientific	
ChemiDoc™ MP Imaging system	Bio-Rad	
Thunder microscope	Lyca microsystems	
Odyssey M	Li-Cor	

Software

GraphPad Prism 9		
Snapgene		
Peaks		
FIJI		

2.2 Methods: Experimental models

2.2.1 Bacterial strain

Wild type *Escherichia coli (E.coli)* strain stable 3 are produced by the lab it selves. They were grown on Luria-Bertani (LB) agar plates with ampicillin (20 ml of 5 g/l yeast extract, 10 g/l peptone from casein, 10 g/l sodium chloride, 12 g/l agar-agar and 100 µg/ml ampicillin) (LB plates (+ A)) at 37°C overnight. The bacteria were also grown in LB medium with ampicillin (10 g/l tryptone,10 g/l sodium chloride, 5 g/l yeast extract, 100 µg/ml ampicillin) (LB medium (+ A)) while shaking at 37°C overnight.

2.2.2 Cell culture

The Flp-In™ T-REx™ 293 PLN_WT and PLN_R14del (HEK_Trex PLN_WT and HEK_Trex PLN_R14del) were generated by Jort van der Geest and cultured in Dulbecco's Modified Eagle Medium (DMEM) with 10% FBS at 37% in a 5% CO_2 atmosphere. The iPSC-CMs were reprogrammed from blood monocytes using the CytoTuneTM-iPS 2.0 Sendai Reprogramming Kit (ThermoFisher, Waltham United states of America). The D4 (PLN_R14del, derived from: Male, 52 years old) C31 (corrected PLN_R14del, used as

isogenic control), and NPO (PLN_WT derived from: Male 31 years old) iPSC-CMs were cultured in Roswell Park Memorial Institute (RPMI) medium with 10% Knock out serum (KOSR) and B27 supplement in a 5% CO_2 atmosphere.

2.3 Methods: Experimental procedures

2.3.1 Llama immunization
Llama immunization was performed by QVQ (Utrecht, the Netherlands). The llama was immunized at day 0, 14, 28, and 35 via injection with PLN_WT and PLN_R14del RNA encapsulated in lipid nanoparticles. Llama blood was collected at day 0, 28 and 43 after the first RNA injection and the serum was isolated.

2.3.2 Detection of nanobodies in llama serum
To detect the presence of PLN_WT and PLN_R14del nanobodies in the serum, an enzyme-linked immuno sorbent assay (ELISA) was performed. WT_PLN, PLN_R14del and CD7 protein were diluted (1 µg/ml) in phosphate-buffered saline (PBS). A 96 wells plate is coated with 60 µl of the diluted proteins and stored on a shaking plate in the cold room (4°C) overnight. The next day, the wells were washed three times with 0.1% PBS-Tween 20 (PBS-T). The wells were blocked with 100 µl 2% Bovine Serum Albumin (BSA) on a shaking plate by room temperature (RT). After 1 h, the wells were incubated with 60 µl llama serum of day 0, 28, or 43 (diluted 1:800) or PBS-T (negative control) for 2 h on the shaking plate by RT. All wells were washed four times with PBS-T and incubated with 100 µl rabbit-anti-llama-immunoglobulin_G-VHH-Horseradish_Peroxidase (rabbit-anti-llama-IgG-VHH-HRP) antibody (diluted 1:10000) by RT. After 1 h, the wells were washed four times with PBS-T and 100 µl of TMB substrate was added to develop color. After a couple of minutes sulfuric acid was added to stop the reaction. The plates were centrifuged to remove bubbles, after which the optical density (OD) was measured at 450 nm.

2.3.3 Affinity of VHHB4 and VHHC6 nanobodies
To test the affinity of the VHHB4 and VHHC6 nanobodies recently described in De Genst *et all.* for the PLN_WT and the PLN_R14del proteins an ELISA was performed as described in 2.3.1 ELISA llama plasma. The plate was coated with WT_PLN, and PLN_R14del protein and instead of the llama serum, three different concentrations (1 µg/ml, 5 µg/ml, and 10 µg/ml) of the two nanobodies were used. The wells were incubated with 100 µl of rabbit-anti-llama-IgG-VHH-Fluorescent (diluted 1:10000) at RT in the dark. After 1 h, the wells were washed three times with PBS-T and incubated with 100 µl of Goat-anti-rabbit-HRP antibody (diluted 1:10000). This is continued as described in 2.3.1 ELISA llama plasma.

2.3.4 Amplification and purification of VHHB4_VHL sequence
The VHHB4_VHL sequence (Supplemental table 1) and the VHHB4 forward and reverse primer were centrifuged at 6000 x G at 4°C for 1 min. 20 µl of nucleases free water was added to the VHHB4_VHL construct followed by a 10x dilution in nucleases free water. The primers were diluted with nucleases free water to a concentration of 100 µM, followed by a 1 min vortex. The polymerase chain reaction (PCR) mix was created by adding 10x Taq buffer, 2 µl of 2.5 mM deoxyribose nucleoside triphosphate (dNTP) mix, 1.5 µl of Magnesium chloride (MgCl₂), 1.25 µl of Dimethyl sulfoxide (DMSO), 0.15 µl Taq polymerase, 2.5 µl of primer mix (10 µM forward primer and 10 µM reverse primer), 1 µl of VHHB4_VHL construct (20 ng) in a total volume of 25 µl. The PCR program was: 95°C for 3 min; 35 cycles of 95°C for 30 sec, annealing temperature (60°C), 72°C for 1 min; 72°C for 10 min, and 4°C for infinite. 6x tritrack was added to 25 µl PCR product and had run on a 1% electrophoresis gel (50 ml (Tris base, acetic acid and EDTA) TAE buffer, 5 µl (Z)-4-((3-Methylbenzo[d]thiazol-2(3H)-ylidene)methyl)-1-propylquinolin-1-ium 4-methylbenzenesulfonate (SYBR safe), and 0.5 g agarose) for 0.5 h at 120 V. The band of the construct was cut out of the gel and purified with the use of the nucleospin PCR clean up kit.

2.3.5 Create empty pHAGE2 vector

2 μg of lentiviral backbone-pHAGE2-PuroR_MCS vector was added to 10x Cutsmart and 40 units of NotI and BamI High Fidelity (HF) enzymes in a total volume of 50 μl. This solution was incubated at 37°C for 1 h after which heat inactivation (65°C) was performed for 20 min. 6x tritrack was added to the empty vector and ran on a 1% electrophoresis gel (50 ml Tris-acetate-Ethylenediaminetetraacetic-acid (TAE) buffer, 5 μl SYBR safe, and 0.5 g agarose) for 0.5 h at 120 V. The band was cut out of the gel and purified with the use of the nucleospin PCR clean up kit. 2x HiFi Master mix was mixed with 0.05 pmol VHHB4_VHL and 0.05 pmol empty lentiviral backbone-pHAGE2-PuroR_MCS vector and was incubated for 15 min at 50°C.

2.3.6 Clonal production of VHHB4_VHL plasmid

50 μl of stable E3 *E. coli* was thawed on ice for 15 min, transfected with 1 μl of the VHHB4_VHL HiFi mix and incubated for 30 min. After 30 sec in the water bath of 42°C, the bacteria were put on ice again for 2 min. After adding 950 μl of LB medium, the bacteria were incubated at 37°C in the shaking incubator. 1 h later, the bacteria were centrifuged at 3000 x G at RT for 1 min and 850 μl of medium was removed. The bacteria were spread over LB agar plates (+ A), and incubated at 37°C. The next day, single bacteria colonies were picked and incubated in 1 ml LB medium (+ A) in the shaking incubator at 37° overnight. The day after, the plasmid of each sample was isolated with the use of the Nucleospin plasmid quickpure kit.

2.3.7 Sanger sequencing of constructs after clonal production

Before preparing the samples for the sequencing, the EF1a_seq_F1 primer (Supplemental table 1) is 10x diluted in RNA free water. 9 μl of the produced plasmid was mixed with 1 μl of the 10x diluted EF1a_seq_F1 primer and send to Macrogen Europe (Amsterdam, The Netherlands) for the performance of the sanger sequencing.

2.3.8 Expanding quantity of VHHB4_VHL plasmid

After the sanger sequencing, a sample with the correct sequence was chosen to produce a larger quantity. 50 μl of stable E3 *E. Coli* bacteria was transfected with 1 μl of the selected plasmid as described in 2.3.6 clonal production of VHHB4_VHL plasmid. 100 μl of non-centrifuged bacteria was spread over a LB agar plate (+ A). The next day, single bacteria colonies were picked and incubated in 300 ml LB medium (+ A) in the shaking incubator at 37°C overnight. The plasmid was isolated with the use of the Xtra Maxi Plus EF kit. Instead of loading the whole lysate onto the column, the precipitate was removed by a 5 min centrifuge at 6000x g to prevent clogging of the filter. The washing with the filter wash Buffer FIL-EF was omitted during the maxi prep. The VHHB4_VHL plasmid was 10x diluted in RNA free water and sent for sanger sequencing as described in 2.3.7 Sanger sequencing of constructs from clonal production.

2.3.9 HEK_Trex cell culture and transfection

500.000 HEK_Trex PLN_R14del or HEK_Trex PLN_WT cells were seeded in DMEM (10% FB, - P/S, and 0.5 μg/ml doxycycline) in each well of a 6-wells plate. Of each of the cell lines, one well is kept as a baseline and did not get any further treatment. Transfection was performed according to manufactures protocol of the Lipofectamine 3000 kit, in short: each of the VHHB4 (provided by Mark Daniels) or VHHB4_VHL plasmid concentration (0.5 μg, 2.5 μg and 5 μg) was mixed with 125 μl Optimem and 4 μl P3000 reagent. 125 μl Optimem was mixed in a different tube with 4 μl lipofectamine 3000. These two tubes were mixed and incubated for 15 min at RT. The DMEM (10% FBS, -P/S, and 0.5 μg/ml doxycycline) of the cells was replaced and the plasmid transfection mix was added to HEK_Trex PLN_WT cells and HEK_Trex PLN_R14del cells. 24 h after transfection the DMEM (10% FBS, -P/S) of all the cells is replaced for new DMEM (10% FBS, - P/S). Each of the wells which are not the baseline or did not get a transfection mixture got either MG132 (dissolved in DMSO) or chloroquine in 2 μM or 10 μM, all wells got the same concentration of DMSO. After optimalization, the

HEK_Trex PLN_R14del and HEK_Trex PLN_WT were transfected with 2.5 µg of VHHB4_VHL or VHHB4 with the use of the same kit. 0.5 µM of MG132 is added to half of the cells, and the other half of the cells received the same concentration of DMSO. To select the successfully transfected cells, a puromycin treatment (1:1000) is used 24 h after transfection.

2.3.10 Lysation of the HEK_Trex cells

Three days after transfection, the cells were detached with the use of 500 µl Trypsin/EDTA diluted in 2.5 ml DMEM (10% FBS, - P/S) and transferred to a 15 ml tube. This is followed by centrifuge (350 x G, 5 min). Next, they were washed with ice cold PBS and once again centrifuged (350 x G, 5 min). Followed up by the lysation of the cells with 500 µl ice cold 1x Radioimmunoprecipitation assay (RIPA) buffer. After 15 min, the cell lysate was transferred to an Eppendorf tube and centrifuged (10.000 x G, 15 min, 4°C). The supernatant was transferred to a new Eppendorf tube.

2.3.11 iPSC-CMs culture and transfection

1.500.000 PLN_WT, PLN_R14del, or isogenic control iPSC-CMs were seeded in RPMI (B27, 10% KOSR and Rock inhibitor(1:1000)) in each well of a 6-well plate. Of each of the cells, one well is kept as a baseline and did not get any further treatment. The transfection of the iPSC-CMs was performed as described in 2.3.9 HEK_Trex cell culture and transfection. The used medium is RPMI (10% KOSR and B27) for the first 24 h after which it was replaced for RPMI (10% FBS and B27). Next to the transfection with VHHB4 and VHHB4_VHL, during the optimization a transfection with the siRNA is also performed with the use of the lipofectamine RNAiMax kit. In short: 9 µl of Lipofectamine RNAiMAX Reagent is mixed with 150 µl Opti-MEM Medium, 30 pmol is diluted in 150 µl Opti-MEM Medium. The two tubes are mixed, incubated for 5 min at RT, and added to the cells.

2.3.12 Viability assay of iPSC-CMs

To determine the viability of the iPSC-CMs an AlamarBlue assay is performed on one of the wells of each condition. Therefore 1 part AlamarBlue is diluted in 9 parts RPMI (+ B27) and filtered through a 0.22 µm syringe filter. The medium is taken off, the iPSC-CMs are washed with RPMI (+ B27) and incubated with 2 ml AlamarBlue at 37°C in the dark. A background measurement is taken along. After 1 h, 100 µl aliquots are taken off, added to a new 96 well plate in duplo and the fluorescence is measured: excitation/emission wave lengths 530/590 nm. After taken off the aliquots, the iPSC-CMs were washed with ice cold PBS and lysed with 500 µl of ice cold 1x RIPA buffer. After 5 min the cells in the RIPA buffer were transferred to a new Eppendorf tube, centrifuged (10.000 x G, 15 min, 4°C), and the supernatant was transferred to a new Eppendorf tube.

2.3.13 Ca^{2+} handling of iPSC-CMs

The other well of the condition is used to perform the Ca^{2+} imaging. Therefore 2 µl Cal520AM (2.5 mM stock) and 4 µl 10% F127 pluronic are mixed well and added to 2 ml Fluor bright (dissolved in DMEM Media). Half of the medium was taken off and replaced with the same amount of Cal520 mix. After incubation of 1 h at 37°C, three recordings per single well were made with the use of the Thunder microscope. Then the wells are washed with PBS and incubated with 4% PFA to fixate the cells. After 20 min PBS is added to the wells and is replaced for new PBS.

2.3.14 Bicinchoninic acid (BCA) assay

The lysates of the HEK_Trex and iPSC-CM samples were five times diluted in PBS and 50 µl of each sample was in duplo loaded on a 96 well plate. A standard curve is created in triplo (50 µl per well) by diluting different concentrations of BSA in 2% RIPA in PBS (400 µg/ml, 200 µg/ml, 100 µg/ml, 50 µg/ml, 25 µg/ml, 12.5 µg/ml, 6.25 µg/ml, 3.125 µg/ml, 1.5625 µg/ml and 0 µg/ml). 50 µl of Working agent (25 parts of reagent A, 24 parts of reagent B and 1 part reagent C) is added to each well. The plate is incubated at 37°C for 1 h and measured with a plate reader at 570 nm.

2.3.15 Protein analysis

1 to 2 μg of protein is diluted in 1x RIPA buffer to get a total volume of 20.8 μl of sample. This is mixed with 10X NuPage LDS Reducing agent and 4X NuPage LDS sample buffer to get a total volume of 32 μl. The samples are heated for 10 min at 95°C and loaded on the Bolt™ 4-12% Bis-Tris Plus gel. The SDS-PAGE is performed at 200 V for 32 min. The gel is transferred to a membrane with the iBlot 2 according to the manufactures protocol. The membrane is blocked with 1:1 licor : Tris-Buffered Saline (TBS) for 1 h at RT. The membrane is incubated with Goat-anti-PLN antibody and Mouse-anti-beta-tubulin (1:1000) diluted in 1:1 0.1% TBS-Tween 20 (TBS-T) : licor and incubated overnight at 4°C. The next day, the primary antibody is removed, and the membrane is washed three times with TBS-T for 15 min. Donkey-anti-goat IrDye 800 and Donkey-anti-mouse IrDye 680 (1:10000 diluted in 1:1 TBS-T : licor) is added to the membrane and incubated at RT in the dark. After 1 h, the membrane is washed three times with TBS-T and one time with TBS for 15 min.

2.3.16 Data analysis

Western blot analysis is performed with the use of FIJI. Thereby the PLN expression was normalized for the beta-tubulin expression. The Cal520 analysis is performed using FUJI and peaks. The sanger sequencing data was analyzed for alignment using snapgene. The rest of the data is analyzed with the use of graphpad Prism 9 software. The following stars are used to visualize the P-value in the figures *: $p < 0.05$, ***: $P < 0.001$, ****: $p < 0.0001$.

3. Results

3.1 No PLN_WT and PLN_R14del nanobodies present in the llama serum

The llama was four times injected with lipid nanoparticles encapsulated with an RNA sequence encoding for wildtype and R14del PLN to generate nanobodies of the heavy chain only antibodies. At three time points after immunization, blood was drawn of which the serum was isolated. This serum was tested for the presence of nanobodies with the use of an ELISA, whereby an increased OD means an increased affinity of the serum for the protein. Coating the plate with a control protein (CD7) showed a significant increase in affinity over time, which means that the immunization of the lama for the control protein was successfully (Figure 3A). However, there was no significant increase of affinity between day 0 and day 28 or day 43 for the PLN_WT and the PLN_R14del protein (Figure 3B and C). Moreover, the overall affinity for PLN_WT and PLN_R14del was very low. This suggests that the immunization of the llama for both proteins was unsuccessful, and that the llama did not produce nanobodies for the PLN_WT and PLN_R14del proteins.
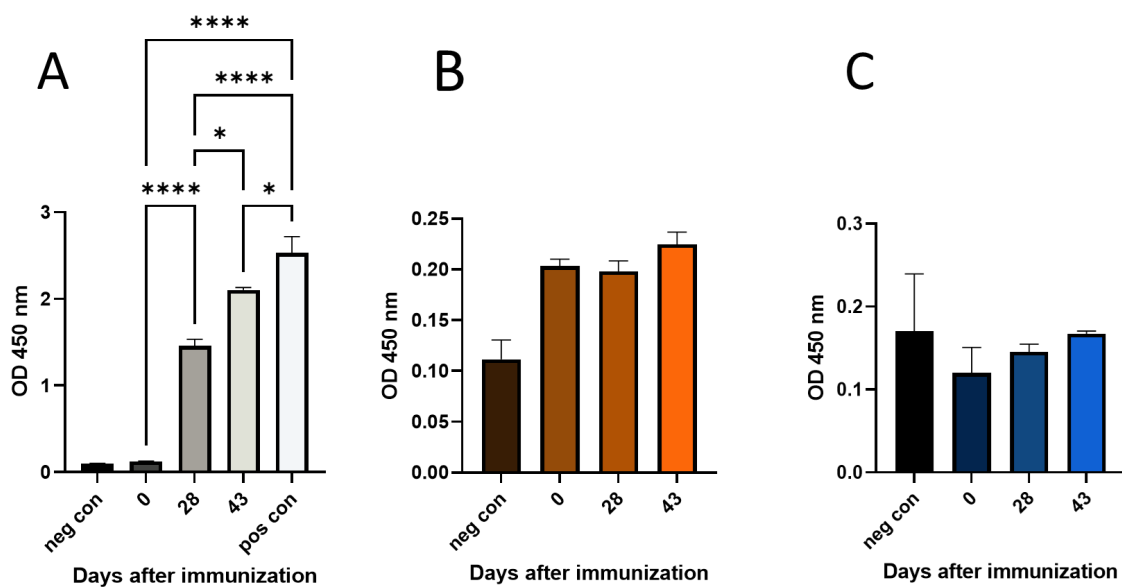
Figure 3 No detection of nanobodies in llama serum 0, 28, and 43 days after immunization with control protein RNA, PLN_WT RNA, and PLN_R14del RNA in lipoparticles. A: Llama serum test of the control protein. For the positive control an antibody for the control protein is used. B: Llama serum test of the PLN_WT protein C: Llama serum test of the PLN_R14del protein.

3.2 VHHB4 has affinity for PLN_WT and PLN_R14del

Since the llama immunization did not result in nanobodies, we decided to test the affinity of the synthetically produced VHHB4 and VHHC6 nanobodies for PLN_WT and PLN_R14del with an ELISA. The different concentrations of the nanobodies (1 µg/ml, 5 µg/ml and 10 µg/ml) were added to wells coated with the PLN_WT and PLN_R14del protein. Increasing the concentration of the VHHB4 showed increased affinity for the PLN_WT as well as the PLN_R14del protein, so the affinity is dosage dependent (Figure 4). Increasing the concentration of the VHHC6 nanobody did not lead to an increase in affinity for PLN_WT or PLN_R14del and the affinity for the proteins was very low. The VHHB4 and VHHC6 nanobodies did not lead to a significant different in affinity between the PLN_WT and PLN_R14del protein, so both nanobodies cannot be used to distinguish the PLN_WT and PLN_R14del protein.
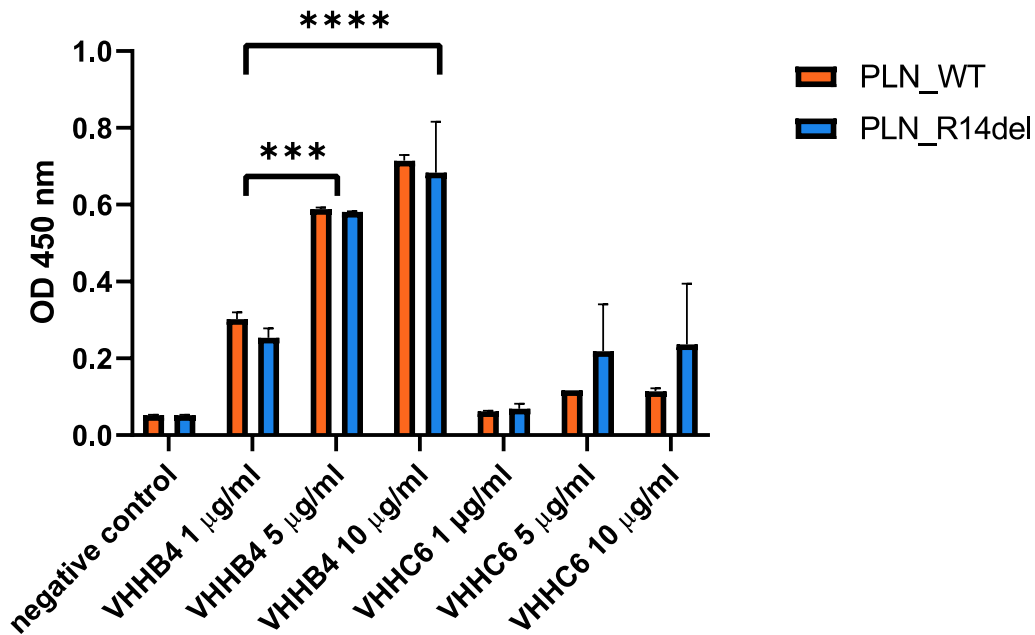
Figure 4 The affinity of VHHB4 for the PLN_WT protein and the PLN_R14del protein. The affinity of VHHB4 and VHHC6 nanobodies for the PLN protein are tested in different concentrations.

3.3 The VHHB4_VHL construct

Because the VHHB4 nanobody has affinity for the PLN_WT and PLN_R14del protein, we determined to order the sequence of a fusion protein of this nanobody with VHL (VHHB4_VHL). This sequence was amplified with a PCR and isolated with a PCR clean-up kit. An empty lentiviral backbone-pHage-2-PuroR_MCS vector was created with the use of restriction enzymes. The VHHB4_VHL sequence was inserted into the empty vector with the use of HIFI assembly. The construct was successfully clonal produced by *E. Coli* bacteria and purified with a maxiprep kit. An overview of the VHHB4_VHl construct inserted in the lentiviral backbone-pHage-2PuroR_MSC can be found in Supplemental figure 1.

3.4 VHHB4_VHL transfection did not result in degradation in HEK_Trex PLN_R14del and HEK_Trex PLN_WT

After a successfully molecular clonation of the VHHB4_VHL sequence we decided to transfect cells to test if the fusion protein is able to reduce the PLN expression. Therefore, the HEK_Trex PLN_WT and HEK_Trex PLN_R14del cells were non-transfected or transfected with the VHHB4_VHL or VHHB4 construct. Their cell lysate was used for protein analysis. The VHHB4 transfection was used to confirm that the effect of the VHHB4-VHL construct was not only due to the nanobody part but also due to the VHL part of the fusion protein. Analysis of the western blots (Figure 5A & C) of HEK_Trex PLN_WT and HEK_Trex PLN_R14del cells showed that some of the VHHB4_VHL transfections in the different concentrations did reduce PLN expression and some not (Figure 5E & G). The 2.5 µg VHHB4 transfection already led to a reduction of the PLN protein in PLN_WT cells and transfection of the same cell type with the VHHB4_VHL construct led to a greater reduction (Figure 5B & F). However, the PLN expression increased in PLN_R14del cells after the same transfection (Figure 5D & H). Addition of 0.5 µM MG132 led to an increase of PLN expression in PLN_WT cells and led to a decrease of PLN expression in PLN_R14del cells. All in all, this data is no clear in the effect of the transfection on the HEK_Trex cells.
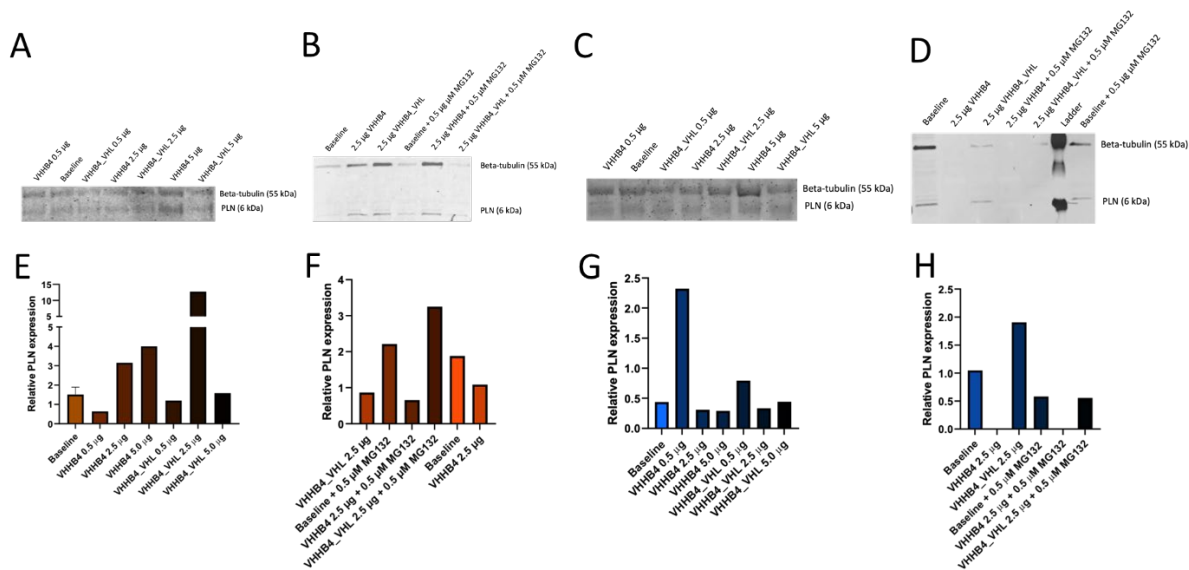
15

Figure 5 No clear effect of transfection in PLN expression in HEK_Trex PLN_WT (orange) and HEK_Trex PLN_R14del (blue).
Western blot of the relative PLN_WT expressing HEK_Trex cells (A & B) and PLN_R14del expressing HEK_T-rex cells (C & D)
after transfection with VHHB4 or VHHB4_VHL. Analysis of the western blot of the PLN_WT expressing HEK_Trex cells (E & F)
and PLN_R14del expressing HEK_Trex cells (G & H).

3.5   No clear reduction of PLN levels observed after VHHB4_VHL transfection of the iPSC-CMs

Although the effect of the transfection in the HEK_Trex cells was not clear, we wanted to check if there was an effect of VHHB4 and VHHB4_VHL transfection in the iPSC-CMs. Besides transfections with those two constructs, we also transfected iPSC-CMs with siRNA as a positive control. To investigate if the transfection with the constructs was not too toxic for the iPSC-CMs an AlamarBlue assay was performed to determine the viability. Transfection with the VHHB4_VHL construct led to an extremely low viability of the cells when selected with puromycin, while without puromycin selection, the iPSC-CMs were much more viable after transfection (Figure 6B, H & N). The transfection with VHHB4 led to a higher viability than transfection with VHHB4_VHL (Figure 6A, G & M). The western blots of the PLN expression are shown in Figure 6C, E, I, K, O and Q. Transfections performed during the optimalisations resulted in a reduced PLN expression in the PLN_WT and isogenic control iPSC-CMs and to an increased PLN expression in PLN_R14del cells (Figure 6D, J & P). 2.5 µg VHHB4 transfection of the isogenic control led to a reduction of PLN expression, while this effect was not observed in the PLN_WT and PLN_R14del (Figure 6F, L & R). The 2.5 µg VHHB4_VHL transfection of PLN_R14del and isogenic control decreased relative PLN expression and increased the relative PLN expression in PLN_WT. Because of the contradicted data of the PLN expression after transfection, it not possible to draw any conclusions of this data.
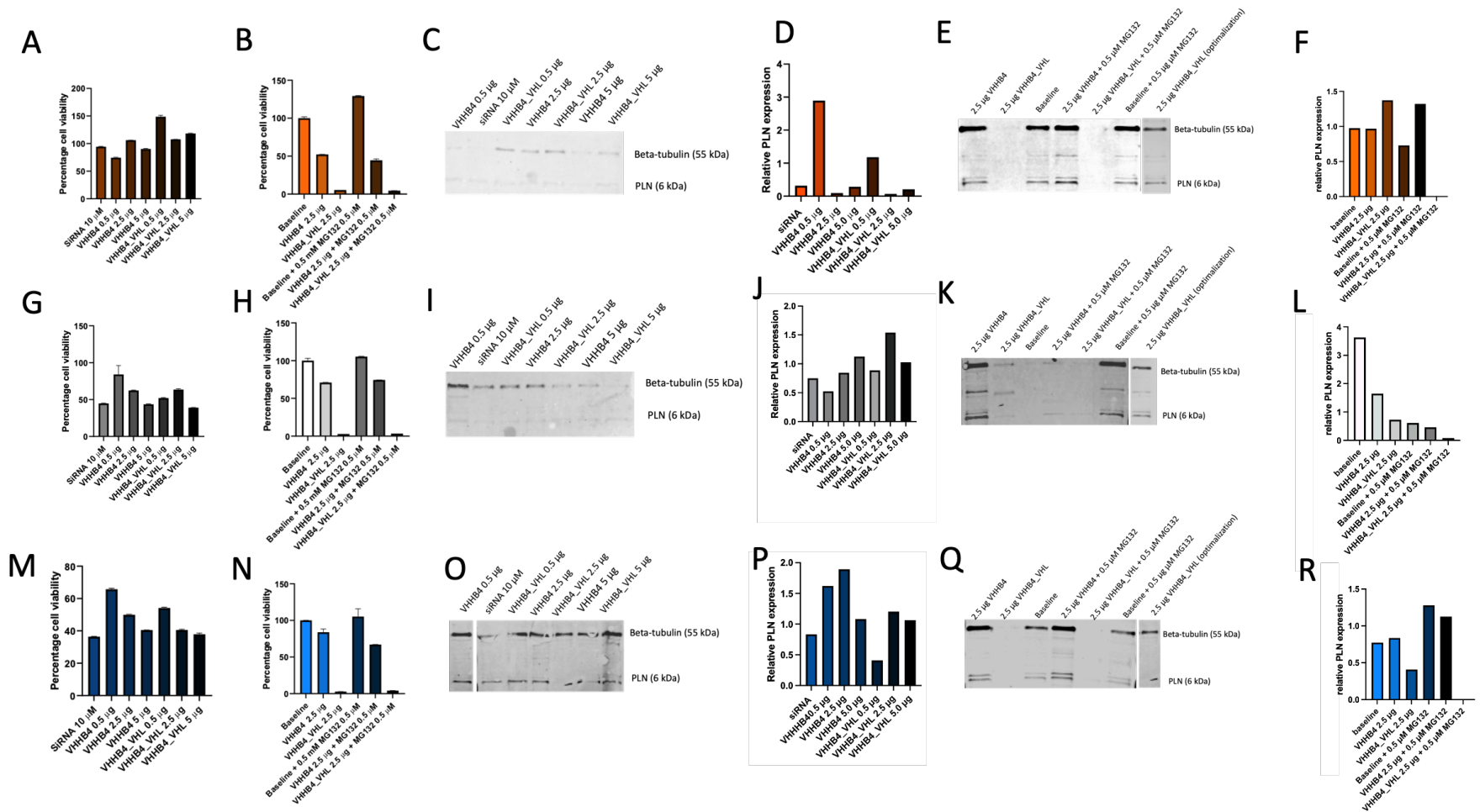
Figure 6 PLN expression of PLN_WT (orange), isogenic control (gray), and PLN_R14del (blue) iPSC-CMs is not clearly reduced after transfection. Viability of PLN_WT (A & B), isogenic control (G & H), and PLN_R14del (M & N) iPSC-CMs after transfection with VHHB4, VHHB4_VHL or siRNA. Western blot of the relative PLN expression of PLN_WT (C & E), isogenic control (I & K) and PLN_R14del (O & Q) iPSC-CMs. Analysis of relative PLN expression of the PLN_WT (D & F), isogenic control (J & L), and PLN_R14del (P & L) iPSC-CMs.

3.6   VHHB4 and VHHB4_VHL had effect on the Ca^{2+} transients of iPSC-CMs

Although the protein analysis showed contradictive data. We still decided to determine the effect of the siRNA, VHHB4 and VHHB4_VHL transfections on the Ca^{2+} transients of the iPSC-CMS with the use of Cal520 incubation. After the incubation, multiple recordings of each well were made with the Thunder. Analyzation of these recordings resulted in the Ca^{2+} transient rise and decay time, beats per minute and the dF/F0 (Ca^{2+} transient amplitude). PLN_WT and PLN_R14del showed a slightly increasing trend in rise time after transfection with the VHHB4_VHL constructs, while this trend was more visible in the isogenic control. The increasing trend in rise time in isogenic control iPSC-CMs was also visible for transfection with VHHB4, while this was not visible for the PLN_WT and PLN_R14del iPSC-CMs. Increasing the concentration of the VHHB4_VHL construct led to an increasing trend in the decay time in the isogenic control and PLN_R14del iPSC-CMs, which was not visible in the PLN_WT iPSC-CMs (Figure 7B, F & J). The transfection of iPSC-CMs with VHHB4 resulted in a decay time all over the place. The beats per minute of all three iPSC-CM types were reduced (Figure 7C, G & K). There seemed to be a trend of decrease of beats per minute for the PLN_WT and PLN_R14del cells after transfection with the VHHB4_VHL construct. Transfection of the isogenic control and PLN_R14del iPSC-CMs did not result in a change of dF/F0, while siRNA, VHHB4 and VHHB4_VHL transfection resulted in a reduction of the dF/F0 in the PLN_WT (Figure 7D, H & L). So, this data showed that the transfections with VHHB4 and VHHB4_VHL had an effect on the Ca^{2+} transient of iPSC-CMs, however it was not clear if the transfection led to an increase or decrease in rise and decay time.
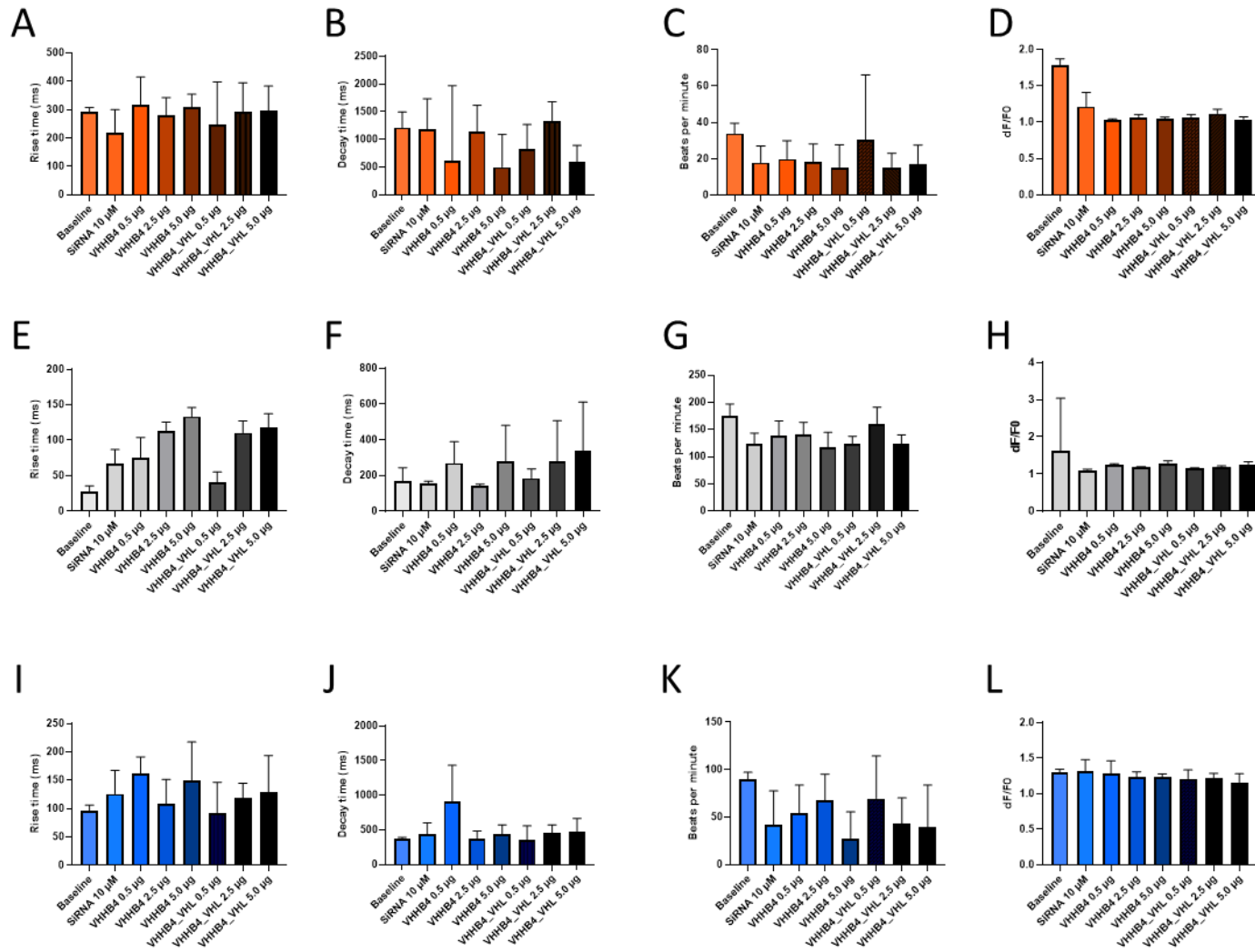
Figure 7 Transfection of the iPSC-CMs with VHHB4 or VHHB4_VHL led to a change of Ca²⁺ transients. Rise time of PLN_WT (A), isogenic control (E) and PLN_R14del (I) iPSC-CMs after transfection with siRNA, VHHB4 or VHHB4_VHL. Decay time of PLN_WT (B), isogenic control (F) and PLN_R14del (J) iPSC-CMs. Beats per minute time of PLN_WT (C), isogenic control (G) and PLN_R14del (H) iPSC-CMs. dF/F0 of PLN_WT (D), isogenic control (H) and PLN_R14del (K) iPSC-CMs.
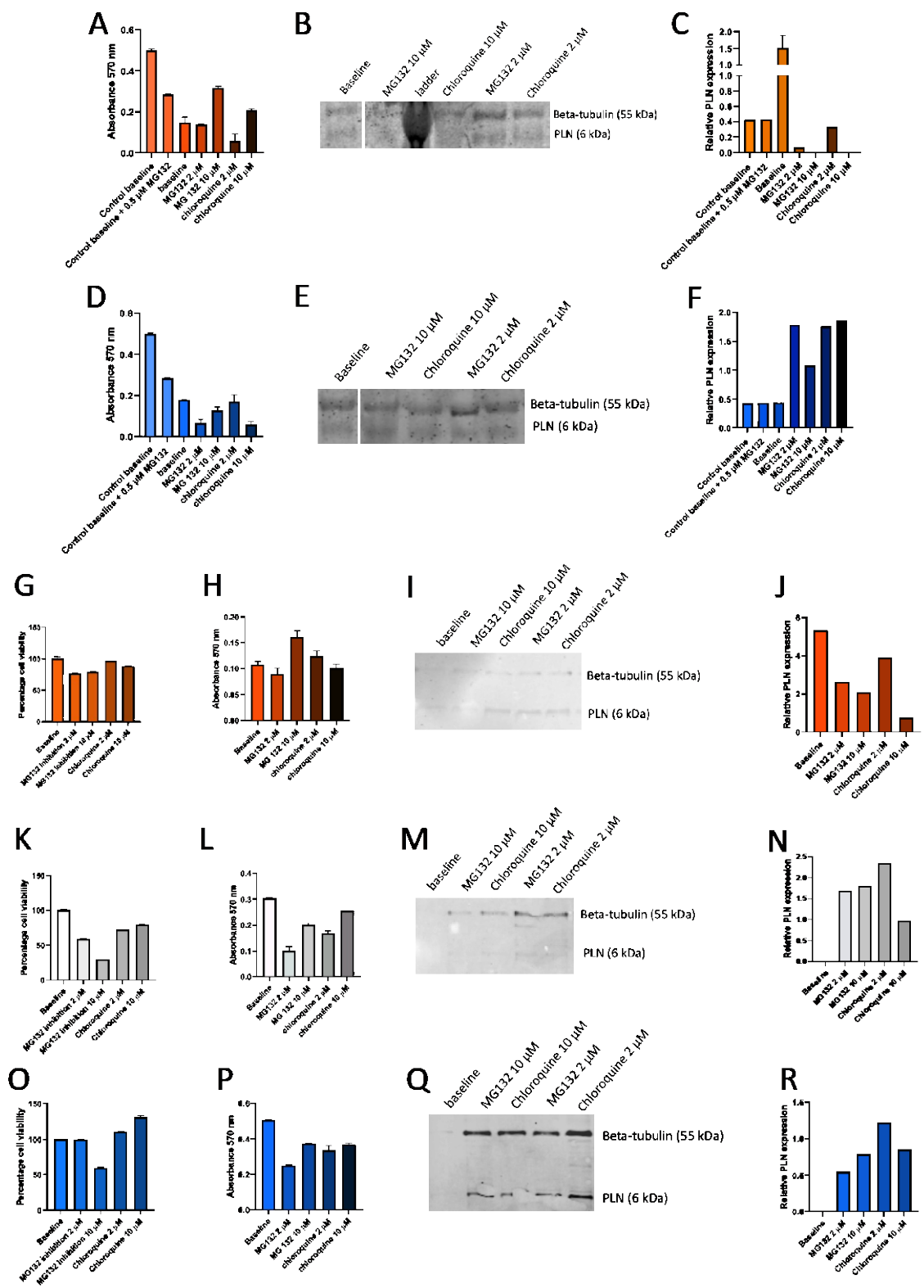
Figure 8 MG132 lead to a reduced viability but the effect of chloroquine and MG132 is not clear. Total protein concentration of the HEK_Trex PLN_WT cells (A) and PLN_R14del cells (D) after treatment with MG132 or chloroquine. Western blot of the HEK_Trex PLN_WT cells (B) and PLN_R14del cells (E). The analysis of the western blot of the PLN_WT (C) and PLN_R14del cells (F). Viability of the. PLN_WT (G), isogenic control (K) and PLN_R14del (O) iPSC-CMS. Total protein concentration of the PLN_WT (H), isogenic control (L) and PLN_R14del (P) iPSC-CMS. Western blot of the PLN_WT (I), isogenic control (M) and PLN_R14del (Q) iPSC-CMS. The analysis of the western blot of the PLN_WT (J), isogenic control (N) and PLN_R14del (R) iPSC-CMS

3.7 MG132 or chloroquine supplementation did not lead to increased protein and PLN expression

Although, the results of the earlier experiments are inconclusive we still wanted to know it the effects we saw came due to the increased activity of the UPS. Therefore, the UPS or autophagy pathway of HEK_Trex cells and the iPSC-CMs was inhibited by respectively MG132 or chloroquine. Increasing the MG132 concentration of HEK_Trex cells led to an increase of total protein concentration (Figure 7A & D). Addition of 10 µM MG132 or chloroquine to the HEK_Trex PLN_WT cells led to a higher total protein concentration than baseline, while in HEK_Trex PLN_R14del the addition of the inhibitors resulted in a lower total protein concentration. Supplementation of MG132 and Chloroquine led to a higher PLN expression in PLN_R14del cells than baseline (Figure 7B & C), while in PLN_WT cells the opposite result was observed (Figure 7E & F).

Adding 2 µM or 10 µM MG132 to the PLN_WT, isogenic control, and PLN_R14del iPSC-CMs led to a reduced viability of the cells (Figure 7G, K & O). This reduction of viability was not observed after the addition of the chloroquine. The supplementation of 2 µM or 10 µM MG132 and chloroquine to iPSC-CMs led to a reduction of the total protein concentration (Figure 7H, L & P). Moreover, in PLN_WT iPSC-CMs both MG132 and chloroquine resulted in a reduction of PLN expression (Figure 7I & J). In the isogenic control and PLN_R14del iPSC-CMs, MG132 decreased the PLN expression more than the chloroquine (Figure 7M, N, Q & R). Just like all earlier shown data, this protein analysis data is inconclusive.
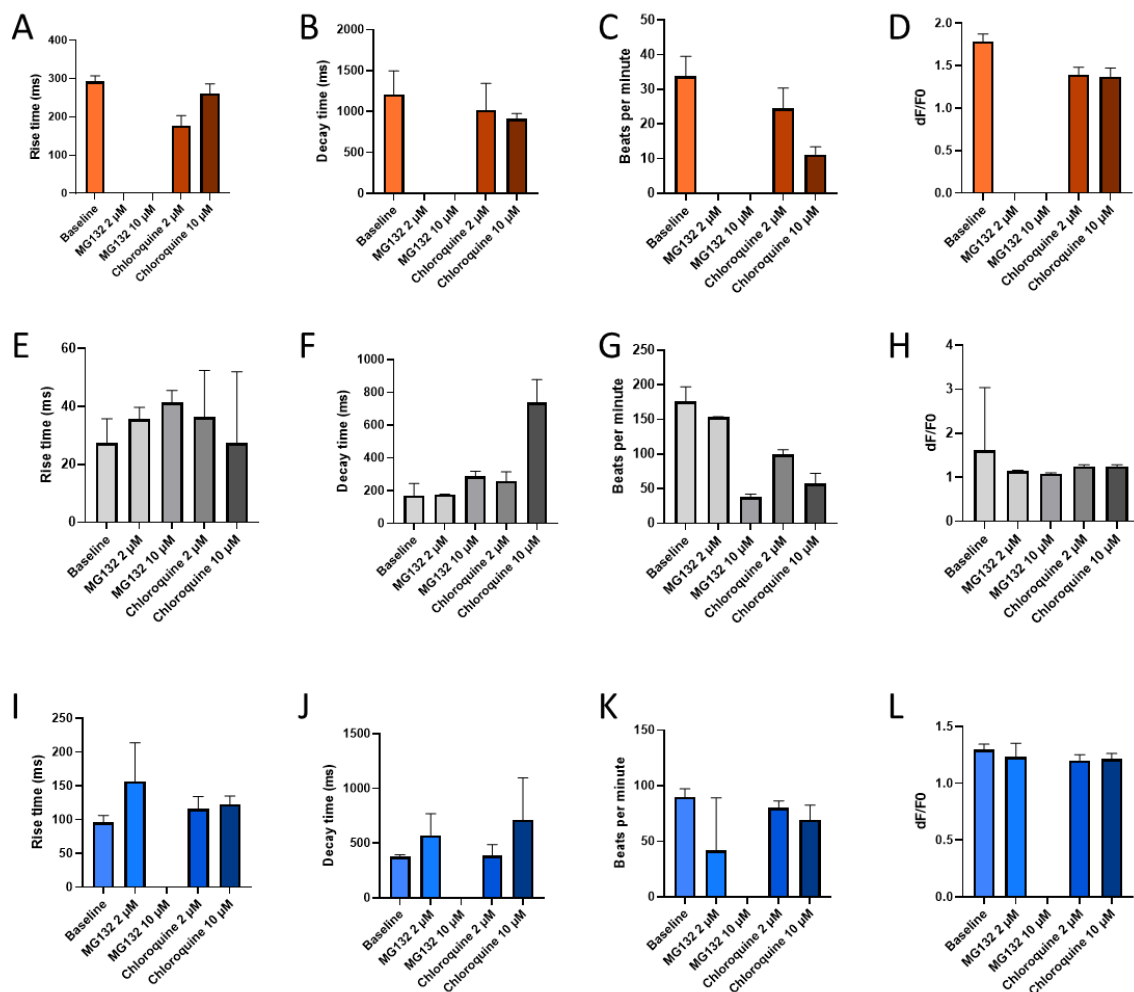

Figure 9 Ca^{2+} transients change upon MG132 or chloroquine treatment. *Rise time of PLN_WT (A), isogenic control (E) and PLN_R14del (I) iPSC-CMs. Decay time of PLN_WT (B), isogenic control (F) and PLN_R14del (J) iPSC-CMs. Beats per minute time of PLN_WT (C), isogenic control (G) and PLN_R14del (H) iPSC-CMs. dF/F0 (Ca^{2+} transient amplitude) of PLN_WT (D), isogenic control (H) and PLN_R14del (K) iPSC-CMs.*

3.8   MG132 and chloroquine have effect on the Ca^{2+} transients of iPSC-CMs

Although, the protein analysis of the iPSC-CMs was indecisive, we still wanted to know if inhibition of the UPS or autophagy pathway of iPSC-CMS led to a change in the functionality. Therefore, the Ca^{2+} transients were analyzed. PLN_WT iPSC-CMs did not show any Ca^{2+} transient when they were treated with 2 µM or 10 µM MG132. Moreover, the PLN_R14 del iPSC-CMs did not show any Ca^{2+} transient in presence of 10 µM MG132. In isogenic control, addition of 2 or 10 µM MG132 or chloroquine led to an increase of the rise time and the same results were observed after addition of 2 µM MG132 to the PLN_R14 del cells (Figure 8A & E). In the PLN_WT and PLN_R14del, the addition of 2 or 10 µM chloroquine led to a decrease of rise time (Figure 8E, I). The decay time seemed to increase due to supplementation of MG132 or chloroquine in the isogenic control and PLN_R14del, while it seemed to decrease in the PLN_WT iPSC-CMs (Figure 8B, F & J). Addition of MG132 or chloroquine led to a reduction in the beats per minute (Figure 8C, G & K). It did not result in a change of dF/F0 (Figure 8D, H & L). All in all, this data showed that MG132 increased the rise and decay time and MG132 and chloroquine reduced the beats per minute. The data was not clear in the effect of chloroquine on the rise and decay time.

4. **Discussion and conclusion**

This report showed that the immunization of a llama with PLN_WT and PLN_R14del protein failed. Moreover, we showed that the VHHB4 nanobody has the same affinity for the PLN_R14del and the PLN_WT protein. We confirmed that the VHHC6 nanobody is unable to bind to unphosphorylated PLN_WT protein, moreover we showed that this nanobody is unable to bind to the unphosphorylated PLN_R14del protein. Furthermore, we were able to produce the VHHB4_VHL fusion protein, which we have tested in HEK_Trex and iPSC-CMs expressing the PLN_WT and PLN_R14del protein. The data about the effect of VHHB4 and VHHB4_VHL transfection on PLN expression of the HEK_Trex cells and iPSC-CMs was all over the place and therefore inconclusive. The functionality data showed a change in Ca^{2+} transient, but it is no clear increase or decrease of the rise and the decay time.

The analysis of llama serum showed absence of PLN nanobodies in the llama serum. The PLN protein is highly conserved among different species[3,8], while the control (CD7 protein) is not[40]. The absence of PLN nanobody is thus most likely due to the similarity of the PLN protein. This result suggests us that proteins which are highly conserved among species are not suitable for llama immunization. Therefore, it is advised that nanobodies against these proteins would be produced synthetically by adapting the recognition domains of already existing nanobodies.

The nanobody affinity assay showed that VHHB4 was able to bind to PLN_WT and PLN_R14del protein with the same affinity. Therefore, the VHHB4 nanobody cannot be used to specifically target the PLN_R14del protein without affecting the PLN_WT protein. Consequently, it cannot be fused to our E3 ligase if we only want to degrade the PLN_R14del protein in heterozygote PLN_R14del cells. Since VHHB4 can recognize the PLN_WT protein and the PLN:SERCA2a ratio is increased during heart failure[7], VHHB4 can potentially be used to target and reduce the PLN concentration in heart failure patients. Moreover, algorithms can possibly be used to identify the bindings site of the VHHB4 nanobody on the PLN protein[41]. If this binding site is near the 14th amino acid, an error prone PCR can be performed. This results in a library of nanobodies[42], which can be analyzed to select a nanobody specifically for PLN_R14del protein. This PLN_R14del specific nanobody can then be used to select the PLN_R14del protein in heterozygote models.

Our affinity assay also showed that VHHC6 was not able to bind to PLN_WT and PLN_R14del protein. Research shows that VHHC6 has only affinity for the phosphorylated PLN_WT conformation[33]. In our assay, the unphosphorylated PLN_WT and PLN_R14del protein are used of which the VHHC6 is not able to bind. In the future, it would be interesting to test the affinity of the VHHC6 nanobody for the phosphorylated PLN protein, especially the PLN_R14del mutated protein would be interesting since this is not tested yet. Literature shows that the PLN_R14del protein cannot be phosphorylated at Ser16, resulting in the expectation that the VHHC6 nanobody would not be able to bind to PLN_R14del protein[43]. If VHHC6 is indeed not able to bind to the PLN_R14del protein, this nanobody can be used to easily distinguish the PLN_R14del protein and the PLN_WT protein during, for example a western blot.

We were able to successfully produce the VHHB4_VHL fusion protein. However, it is not known which E3 ligase plays the key role in cardiomyocytes, and therefore it would be interesting to also produce other fusion protein(s) of VHHB4 and an E3 ligase. In that way you can test multiple fusion proteins and test which one works the best for the degradation of the PLN protein. After the production of the VHHB4_VHL fusion protein, we transfected HEK_Trex cells and iPSC-CMs with our fusion protein to test whether the fusion protein is able to degrade the PLN protein or not.

Our results of the PLN protein of HEK_Trex PLN_WT and HEK_Trex PLN_R14del after transfection with eighter VHHB4, VHHB4_VHL or siRNA analysis were inconclusive with each other and are not completely as expected. This inconclusiveness is also observed in the transfected PLN_WT, isogenic control, and PLN_R14del iPSC-CMs. The total protein concentration and PLN concentration after chloroquine or MG132 supplementation to HEK_Trex PLN_WT and HEK_Trex PLN_R14del showed contradictory results. The same contradiction is observed after addition of chloroquine and MG132 to

the PLN_WT, isogenic control, and PLN_R14del iPSC-CMs. There are several possibilities why our results are not as expected.

First, the total protein concentrations of the cell lysates were very low, which resulted in low signals on the western blot. These signals are hard to analyze and are more likely to have a high standard deviation. There are multiple solutions to increase the protein concentration of cell lysates and thereby increase the western blot signal, such as addition of protease or phosphatase inhibitors to prevent the unwanted degradation, make multiple aliquots to reduce the number of freeze-thaw cycles to prevent protein degradation or use less (RIPA) buffer[44].

Second, the sample size was only one, since we have performed the experiments only once. Hence, it is not known if the loading process of the gel also lead to differences/ absence of signal. This means that the differences could also be created by the technical issues or because of the standard deviation between samples. Therefore, it is suggested to repeat the experiments with multiple wells for each condition to have a larger sample size and thereby have a lower standard deviation.

Third, the synthetically overexpressed PLN protein concentrations are not as high as you expect. Literature shows that doxycycline has a half-life time of 24 h and that for continues expression of gene of interest the medium should be replaced each 48 h[45]. So, to have a higher PLN expression in the HEK_Trex cells it is suggested to replace the medium every 48 h for medium with new doxycycline.

Fourth, the low transfection efficiency of the lipofectamine 3000 kit is found by analyzing the viability of unselected and selected VHHB4_VHL transfected iPSC-CMs. Puromycin selected VHHB4_VHL transfected iPSC-CMs revealed an extreme reduction in viability, which was not observed in unselected iPSC-CMs. This low transfection efficiency is in accordance with earlier research, which shows an efficiency of 3.7 to 13%[46]. The selection of iPSC-CMs resulted in an extreme low total protein expression, which results in a PLN expression which we could not analyze. To still have the data about the 2.5 µg VHHB4_VHL, the data of the unselected optimization of this group is used. In future it is suggested to use a lentiviral vector transduction resulting in a higher efficiency and therefore more reliable results[47]. For the transfection of the VHHB4, the same transfection kit is used so it is likely that the transfection efficiency of this construct is also very low. This low transfection efficiency should be considered by interpreting the iPSC-CM transfection data.

Degradation of PLN leads to less inhibition of SERCA2a and results in more Ca^{2+} transport to the SR. Therefore, it is expected to see a decrease in the decay time[33,53]. However, our data showed a slightly increase of the decay time. When SERCA2a inhibition is reduced due to absence of PLN, it will lead to an increased rise time. After all, SERCA2a will pump the Ca^{2+}, which already left the SR via the RYR, back to the SR[6,53]. Therefore, it will take more time to get all the Ca^{2+} out of the SR. This increase in rise time was observed in isogenic control and PLN_R14del iPSC-CMs, but not in the PLN_WT iPSC-CMs. However, by looking to the Ca^{2+} data, we still need to take in account that the iPSC-CMs had a very low transfection efficiency and that the sample size was only one. So, the observed differences can be caused by standard deviation instead of the effect due to transfection with the fusion protein.

Addition of MG132 to iPSC-CMs led to a disturbed Ca^{2+} handling, which can be seen in the absence of Ca^{2+} transients in the isogenic control (2 and 10 µM MG132) and PLN_R14del (10 µM). Moreover, this effect can be observed in the reduced beats per minute. The effect of MG132 and chloroquine on the decay and rise time was not clear in our data, but there was a disturbance of decay and rise time visible. Research shows that by inhibition of the proteasome, the autophagy pathway will take over. This will lead to myofiber disarray and thereby a disturbed Ca^{2+} handling[50].

In short: we had successfully produced the VHHB4_VHL fusion protein, however we still do not know if this protein is able to perform targeted degradation and thereby improve the Ca^{2+} handling of the cardiomyocytes.

## 5.	Acknowledgement

6.   References

1.   Cheng, H. & Lederer, W. J. Calcium sparks. *Physiol Rev* **88**, 1491–1545 (2008).
2.   Venetucci, L., Denegri, M., Napolitano, C. & Priori, S. G. Inherited calcium channelopathies in the pathophysiology of arrhythmias. *Nature Reviews Cardiology 2012 9:10* **9**, 561–575 (2012).
3.   Stammers, A. N. *et al.* The regulation of sarco(endo)plasmic reticulum calcium-ATPases (SERCA)1. *Canadian Journal of Physiology and Pharmacology* vol. 93 843–854 Preprint at https://doi.org/10.1139/cjpp-2014-0463 (2015).
4.   MacLennan, D. H. & Kranias, E. G. Phospholamban: A crucial regulator of cardiac contractility. *Nature Reviews Molecular Cell Biology* vol. 4 566–577 Preprint at https://doi.org/10.1038/nrm1151 (2003).
5.   Landstrom, A. P., Dobrev, D. & Wehrens, X. H. T. Calcium Signaling and Cardiac Arrhythmias. *Circ Res* **120**, 1969–1993 (2017).
6.   Tham, Y. K. *et al.* Pathophysiology of cardiac hypertrophy and heart failure: signaling pathways and novel therapeutic targets. *Archives of Toxicology 2015 89:9* **89**, 1401–1438 (2015).
7.   Minamisawa, S. *et al.* Chronic Phospholamban–Sarcoplasmic Reticulum Calcium ATPase Interaction Is the Critical Calcium Cycling Defect in Dilated Cardiomyopathy. *Cell* **99**, 313–322 (1999).
8.   Hof, I. E. *et al.* Prevalence and cardiac phenotype of patients with a phospholamban mutation. *Netherlands Heart Journal* **27**, 64–69 (2019).
9.   Kranias, E. G., Doevendans, P. A., Glijnis, P. C. & Hajjar, R. J. PLN foundation: A foundation of patients for patients. *Circ Res* **123**, 1276–1278 (2018).
10.   Haghighi, K. *et al.* Human phospholamban null results in lethal dilated cardiomyopathy revealing a critical difference between mouse and human. *Journal of Clinical Investigation* **111**, 869 (2003).
11.   Truszkowska, G. T. *et al.* A study in Polish patients with cardiomyopathy emphasizes pathogenicity of phospholamban (PLN) mutations at amino acid position 9 and low penetrance of heterozygous null PLN mutations. *BMC Med Genet* **16**, 1–9 (2015).
12.   Haghighi, K. *et al.* The human phospholamban Arg14-deletion mutant localizes to plasma membrane and interacts with the Na/K-ATPase. *J Mol Cell Cardiol* **52**, 773–782 (2012).
13.   Haghighi, K. *et al.* A mutation in the human phospholamban gene, deleting arginine 14, results in lethal, hereditary cardiomyopathy. *Proc Natl Acad Sci U S A* **103**, 1388–1393 (2006).
14.   Posch, M. G. *et al.* Genetic deletion of arginine 14 in phospholamban causes dilated cardiomyopathy with attenuated electrocardiographic R amplitudes. *Heart Rhythm* **6**, 480–486 (2009).
15.   Cuello, F. *et al.* Impairment of the ER/mitochondria compartment in human cardiomyocytes with PLN p.Arg14del mutation. *EMBO Mol Med* **13**, (2021).
16.   Badone, B. *et al.* Characterization of the pln p.Arg14del mutation in human induced pluripotent stem cell-derived cardiomyocytes. *Int J Mol Sci* **22**, (2021).
17.   Vostrikov, V. V., Soller, K. J., Ha, K. N., Gopinath, T. & Veglia, G. Effects of Naturally Occuring Arginine 14 Deletion on Phospholamban Conformational Dynamics and Membrane Interactions. *Biochim Biophys Acta* **1848**, 315 (2015).
18.   Ceholski, D. K., Trieber, C. A. & Young, H. S. Hydrophobic Imbalance in the Cytoplasmic Domain of Phospholamban Is a Determinant for Lethal Dilated Cardiomyopathy. *J Biol Chem* **287**, 16521 (2012).
19.   Te Rijdt, W. P. *et al.* Myocardial fibrosis as an early feature in phospholamban p.Arg14del mutation carriers: phenotypic insights from cardiovascular magnetic resonance imaging. *Eur Heart J Cardiovasc Imaging* **20**, 92–100 (2019).
20.   Gho, J. M. I. H. *et al.* High Resolution Systematic Digital Histological Quantification of Cardiac Fibrosis and Adipose Tissue in Phospholamban p.Arg14del Mutation Associated Cardiomyopathy. *PLoS One* **9**, (2014).
21.   Doevendans, P. A., Glijnis, P. C. & Kranias, E. G. Leducq Transatlantic Network of Excellence to Cure Phospholamban-Induced Cardiomyopathy (CURE-PLaN). *Circ Res* **125**, 720–724 (2019).
22.   Eijgenraam, T. R. *et al.* The phospholamban p.(Arg14del) pathogenic variant leads to cardiomyopathy with heart failure and is unresponsive to standard heart failure therapy. *Sci Rep* **10**, (2020).
23.   Hassanzadeh-Ghassabeh, G., Devoogdt, N., De Pauw, P., Vincke, C. & Muyldermans, S. Nanobodies and their potential applications. *Nanomedicine (Lond)* **8**, 1013–1026 (2013).

24. Könning, D. *et al.* Camelid and shark single domain antibodies: structural features and therapeutic potential. *Curr Opin Struct Biol* **45**, 10–16 (2017).

25. Muyldermans, S. Nanobodies: natural single-domain antibodies. *Annu Rev Biochem* **82**, 775–797 (2013).

26. Liu, M., Li, L., Duo, J. & Liu, Y. Nanobody-A versatile tool for cancer diagnosis and therapeutics Therapeutic Approaches and Drug Discovery > Nanomedicine for Oncologic Disease. *Wires Nanomedicine and nanobiotechnology* **13**, e1697 (2021).

27. de Marco, A. Recombinant expression of nanobodies and nanobody-derived immunoreagents. *Protein Expr Purif* **172**, 105645 (2020).

28. Wang, Y. *et al.* Nanobody-derived nanobiotechnology tool kits for diverse biomedical and biotechnology applications. *Int J Nanomedicine* **11**, 3287–3303 (2016).

29. Wang, Y. *et al.* Nanobody-derived nanobiotechnology tool kits for diverse biomedical and biotechnology applications. *Int J Nanomedicine* **11**, 3287 (2016).

30. Turner, K. B., Alves, N. J., Medintz, I. L. & Walper, S. A. Improving the targeting of therapeutics with single-domain antibodies. *https://doi.org/10.1517/17425247.2016.1133583* **13**, 561–570 (2016).

31. Salvador, J. P., Vilaplana, L. & Marco, M. P. Nanobody: outstanding features for diagnostic and therapeutic applications. *Anal Bioanal Chem* **411**, 1703–1713 (2019).

32. Bao, G., Tang, M., Zhao, J. & Zhu, X. Nanobody: a promising toolkit for molecular imaging and disease therapy. *EJNMMI Res* **11**, (2021).

33. De Genst, E. *et al.* Blocking phospholamban with VHH intrabodies enhances contractility and relaxation in heart failure. *Nat Commun* **13**, 3018 (2022).

34. Zhao, L., Zhao, J., Kunhong, Z., Tong, A. & Jia, D. Targeted protein degradation: mechanisms, strategies and application. *Signal Transduct Target Ther* **7**, 113 (2022).

35. Shin, Y. J. *et al.* Nanobody-targeted E3-ubiquitin ligase complex degrades nuclear proteins OPEN. *Scientific RepoRts |* **5**, 14269 (2015).

36. Wu, T. *et al.* Targeted protein degradation as a powerful research tool in basic biology and drug target discovery. *Nat Struct Mol Biol* **27**, 605–614 (2020).

37. Békés, M., Langley, D. R. & Crews, C. M. PROTAC targeted protein degraders: the past is prologue. *Nat Rev Drug Discov* **21**, 181 (2022).

38. Conaway, R. C. & Conaway, J. W. von Hippel–Lindau (VHL) Protein. in *Encyclopedia of Biological Chemistry: Second Edition* 570–571 (Academic Press, 2013). doi:10.1016/B978-0-12-378630-2.00333-9.

39. Fulcher, L. J. *et al.* An affinity-directed protein missile system for targeted proteolysis. *Open Biol* **6**, 160255 (2016).

40. Lee, J. Y., Bae, J., Choi, I., Park, C. G. & Chun, T. Molecular cloning and expression analysis of pig CD7. *Vet Res Commun* **38**, 257–263 (2014).

41. Ludington, J. L. Protein binding site analysis for drug discovery using a computational fragment-based method. *Methods in Molecular Biology* **1289**, 145–154 (2015).

42. Mccullum, E. O., Williams, B. a R., Zhang, J. & Chaput, J. C. Error Based PCR Mutagenesis Protocols. *Methods in Molecular Biology* **634**, 103–109 (2010).

43. Vafiadaki, E., Haghighi, K., Arvanitis, D. A., Kranias, E. G. & Sanoudou, D. Aberrant PLN-R14del Protein Interactions Intensify SERCA2a Inhibition, Driving Impaired Ca2+ Handling and Arrhythmogenesis. *Int J Mol Sci* **23**, (2022).

44. Preparing Cell Lysates. https://www.sigmaaldrich.com/NL/en/technical-documents/technical-article/protein-biology/western-blotting/perparing-cell-lysates.

45. Clontech, Laboratories & Inc. Tet-One™ Inducible Expression System User Manual Tet-One Inducible Expression System User Manual.

46. Tan, S. *et al.* Non-viral vector based gene transfection with human induced pluripotent stem cells derived cardiomyocytes. *Sci Rep* **9**, (2019).

47. Sato, Y. *et al.* Disease modeling and lentiviral gene transfer in patient-specific induced pluripotent stem cells from late-onset Pompe disease patient. *Mol Ther Methods Clin Dev* **2**, 15023 (2015).

48. Lee, D. H. Proteasome inhibitors: valuable new tools for cell biologists. *Trends Cell Biol* **8**, 397–403 (1998).

49. Ding, W. X. *et al.* Linking of autophagy to ubiquitin-proteasome system is important for the regulation of endoplasmic reticulum stress and cell viability. *Am J Pathol* **171**, 513–524 (2007).

50. McDermott-Roe, C. *et al.* Investigation of a dilated cardiomyopathy-associated variant in BAG3 using genome-edited iPSC-derived cardiomyocytes. *JCI Insight* **4**, (2019).

51. Teng, A. C. T. *et al.* Metformin increases degradation of phospholamban via autophagy in cardiomyocytes. *Proc Natl Acad Sci U S A* **112**, 7165–7170 (2015).

52. Goversen, B., van der Heyden, M. A. G., van Veen, T. A. B. & de Boer, T. P. The immature electrophysiological phenotype of iPSC-CMs still hampers in vitro drug screening: Special focus on IK1. *Pharmacol Ther* **183**, 127–136 (2018).

53. Badone, B. *et al.* Characterization of the pln p.Arg14del mutation in human induced pluripotent stem cell-derived cardiomyocytes. *Int J Mol Sci* **22**, (2021).

7. Supplemental figures and tables

Supplemental table 1 Overview of the used sequences.

VHHB4 forward primer	aggtgtcgtgaagcggccgc	40
VHHB4 reverse primer	taacgttagggggggggagggat	40
EF1a_seq_F1 sequence primer	gttcattctcaagcctcaga	40
VHHB4_VHL sequence	Atggctagcgaagtgcagctgcaggagagcggcggaggcc	40
	Tagtccaagcaggcgggtctctgcgtctgtcttgcgccgc	80
	Ctcaggattctcattttaccgccacgctatggggtggttc	120
	Cggcaggcccccggcaaagaacgcgaatgggtggccgaaa	160
	Tcgattgggaggggggctacacctattacgccgatagtgt	200
	Gaaagggcggtttacaatttcacgggataacgctaagaac	240
	Accgtgtatcttcagatgaacagtctgaaaccggaagaca	280
	Ctgcagtgtactattgcgcggccggtagggacctgtatgc	320
	Ttattggggtcaggggacgcaggtgaccgtttcctcctct	360
	Agaggcggtggaagcggaggcggttctggcggggggaagcg	400
	Ggggcggctcgactttgccagtatacacactcaaggagag	440
	Atgtctccaagtcgttcgcagtctggtcaagcctgagaat	480
	Tacagacgactcgatatagtaaggtctttatacgaggatt	520
	Tggaggaccatcccaatgttcagaaggacctggagaggct	560
	Tacacaggagagaatcgcacaccaacgaatgggtgacgga	600
	tcatga	660
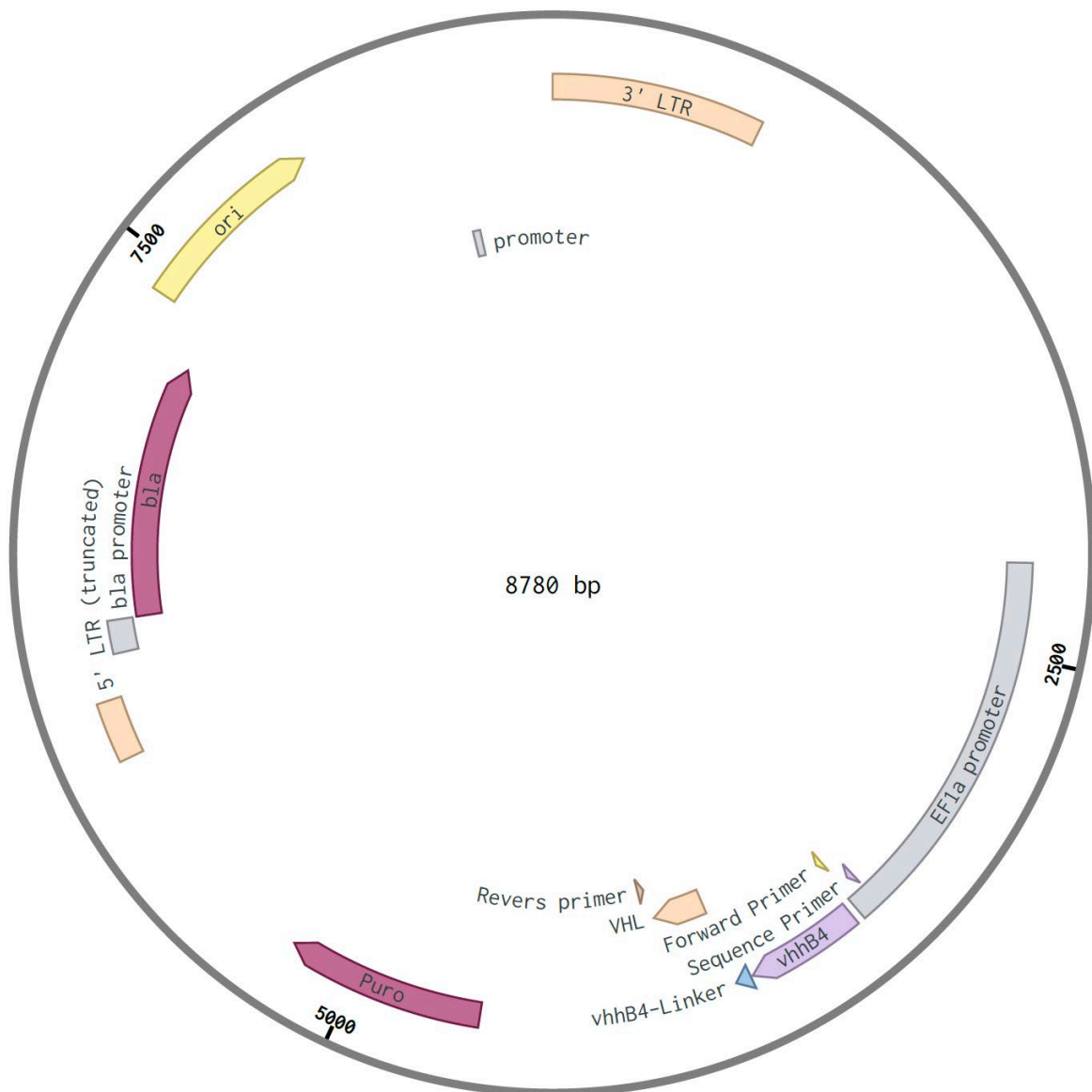
Supplemental figure 1 Overview of the VHHB4_VHL construct. *The construct consists of: a 3' Long terminal repeat (LTR), the elongated factor-1 alfa (EF1a) promotor, Th VHHB4 sequence, VHHB4-linnker sequence , VHL sequence, puromycin resistance gene (Puro), 5' LTR, beta-lactamase (bla) promotor, bla sequence and the origin of replication (ori). The primer used for the sanger sequencing has the same sequence as a part of the EF1a promotor. The forward and reverse primers are used for the PCR of the VHHB4_VHL construct.*